Research Article

Mario Mordmüller*, Viktoria Kleyman, Manuel Schaller, Mitsuru Wilson, Dirk Theisen-Kunde, Karl Worthmann, Matthias A. Müller and Ralf Brinkmann

Towards temperature controlled retinal laser treatment with a single laser at 10 kHz repetition rate

https://doi.org/10.1515/aot-2021-0041
Received August 23, 2021; accepted October 29, 2021;
published online November 22, 2021

Abstract: Laser photocoagulation is one of the most frequently used treatment approaches in ophthalmology for a variety of retinal diseases. Depending on indication, treatment intensity varies from application of specific micro injuries down to gentle temperature increases without inducing cell damage. Especially for the latter, proper energy dosing is still a challenging issue, which mostly relies on the physician's experience. Pulsed laser photoacoustic temperature measurement has already proven its ability for automated irradiation control during laser treatment but suffers from a comparatively high instrumental effort due to combination with a conventional continuous wave treatment laser. In this paper, a simplified setup with a single pulsed laser at 10 kHz repetition rate is presented. The setup combines the instrumentation for treatment as well as temperature measurement and control in a single device. In order to compare the solely pulsed heating with continuous wave (cw) tissue heating, pulse energies of 4 µJ were applied with a repetition rate of 1 kHz to probe the temperature rise, respectively. With the same average laser power of 60 mW an almost identical temporal temperature course was retrieved in both irradiation modes as expected. The ability to reach and maintain a chosen aim temperature of 41 °C is demonstrated by means of model predictive control (MPC) and extended Kalman filtering at a the measurement rate of 250 Hz with an accuracy of less than ±0.1 °C. A major advantage of optimization-based control techniques like MPC is their capability of rigorously ensuring constraints, e.g., temperature limits, and thus, realizing a more reliable and secure temperature control during retinal laser irradiation.

Keywords: extended Kalman filter; laser-coagulation; model predictive control; ophthalmology; photo-acoustics.

***Corresponding author: Mario Mordmüller**, Institute of Biomedical Optics, University of Lübeck, Lübeck, Germany, E-mail: m.mordmueller@uni-luebeck.de
Viktoria Kleyman and Matthias A. Müller, Institute for Automatic Control, Leibniz University Hannover, 30167 Hannover, Germany, E-mail: kleyman@irt.uni-hannover.de (V. Kleyman), mueller@irt.uni-hannover.de (M.A. Müller)
Manuel Schaller, Mitsuru Wilson and Karl Worthmann, Faculty of Mathematics and Natural Sciences, Technische Universität Ilmenau, Ilmenau, Germany, E-mail: manuel.schaller@tu-ilmenau.de (M. Schaller), mitsuru.wilson@tu-ilmenau.de (M. Wilson), karl.worthmann@tu-ilmenau.de (K. Worthmann)
Dirk Theisen-Kunde, Medical Laser Center Lübeck, Lübeck, Germany, E-mail: dirk.theisenkunde@uni-luebeck.de
Ralf Brinkmann, Institute of Biomedical Optics, University of Lübeck, Lübeck, Germany; and Medical Laser Center Lübeck, Lübeck, Germany, E-mail: ralf.brinkmann@uni-luebeck.de

1 Introduction

In retinal treatments, laser photocoagulation has become one of the most frequently used therapeutic methods for diseases such as diabetic retinopathy and macula edema [1, 2], and ischemia due to vein occlusion [3–5]. This method originates from Meyer–Schwickerath who introduced a new approach to stop advancing detachment of the retina by means of intense light in the early 1950s [6]. After the usage of arc lamps, state of the art photo thermal treatment devices comprise lasers, typically in the green spectral range. Depending on the indication, a spot diameter of 50–500 µm and laser power of 50–500 mW is applied for 20–200 ms. The achieved damage to tissue can be estimated by the Arrhenius theory, which relates the temperature increase and irradiation with respect to the induced damage [7].

Since the early days, micro injuries were intended to achieve artificial scar production to prevent retinal detachment; it emerged that also less damaging or even nondamaging laser treatment can have a therapeutic effect, e.g. for central serous retinopathy (CSR) [8]. Here, the effect of laser radiation on cells is mostly unknown, but

the accompanied increase of temperature is assumed to be the dominating one. The laser light is absorbed primarily in the highly pigmented retinal pigment epithelium (RPE), subsequently heating up the irradiated tissue. After exceeding a temperature of approximately 63 °C [9], irradiated spots become visible as whitish lesions due to light scattering induced by thermal protein denaturation in the retina, which is also referred to as (photo-) coagulation. However, irreversible RPE damage already occurs at lower temperatures around 53 °C [10].

The amount of energy required to achieve denaturation strongly depends on fundus absorption, which in turn is governed by the local pigmentation of the RPE and choroid, which separate the retina from the sclera. For CSR, treatment energy is typically selected by the physician according to practical experience and by means of titration. To do so, the laser beam is aimed at the peripheral of the treatment area and laser energy is gradually increased until lesions become ophthalmoscopically visible. This energy is then reduced to roughly 50–70% to ensure subvisible treatment in the relevant areas. Since lesion visibility can, in addition, occur with a delay of up to several hours and pigmentation density can vary to a factor of up to three on a single eye [11, 12], titration still leaves a serious uncertainty. Hence, proper energy dosing is especially difficult and most challenging for sub-damage treatment.

In order to meet the need for proper energy dosing, Brinkmann et al. [13] have developed an approach for online temperature measurement during retinal laser treatment using the photo-acoustic effect. It has already proven its feasibility during animal experiments on rabbits [9, 14] and even in clinical studies [13]. Briefly, if a sufficiently short light pulse from the probe laser is absorbed by the RPE, the impulsive expansion gives rise to a pressure transient, which can be detected at the exterior corneal surface of the eye by means of an ultrasonic transducer. The amplitude of the pressure transient is used to compute a tissue temperature in real time during irradiation with the treatment laser. The opto-acoustically measured temperature is also referred to as the volume temperature since it represents a depth weighted average temperature of the irradiated volume over different layers wherein the absorption takes place. Hence, it is more suitable for temperature control to use the peak temperature as controller input to avoid undesired damage to the tissue. Thus, in [9, 13, 15] an approximated conversion of the volume temperature into the peak temperature was applied.

Open-loop [9] and closed-loop control approaches [16, 17] were executed, thus far, enabling to quickly reach and maintain a certain temperature within the two laser setup. For the closed-loop control, a first-order model based on the approximated peak temperature was identified and a robust H_∞-controller was designed to account for the varying absorption coefficients. Drawbacks of this approach are the use of an offline (and roughly) approximated conversion between peak and volume temperature and a possible lack of performance due to the robust design. To overcome these drawbacks, a joint state and parameter estimation based on the volume temperature was presented in [18]. This also enables sophisticated control design such as model predictive control to further enhance the safety of the treatment.

In this paper, we report on a simplified setup for temperature controlled retinal laser irradiation with just one pulsed 10 kHz laser device, which is used for tissue heating and opto-acoustic temperature measurement simultaneously. The setup is used to demonstrate first the feasibility of using just one laser, and second the superiority of controlled power modulation with 250 Hz over irradiation with fixed laser power, which still is state of the art in clinical application. Furthermore, first results of a model predictive controller in combination with an online parameter and state estimation are shown as a proof of concept for more advanced control strategies.

2 Materials and methods

2.1 Experimental

This section gives an overview of the opto-acoustic temperature measurement technique and the experimental setup. Furthermore, the signal processing and measurement scheme is described in detail and a comparison of pulsed and continuous wave tissue heating is presented.

2.1.1 Opto-acoustic temperature measurement: The principle of opto-acoustic temperature measurement has already been reported in detail by Brinkmann et al. [13] and is only summarized within this section. Upon absorption of a light pulse with a pulse length shorter than the thermal relaxation time, the irradiated tissue undergoes a strong thermo-elastic expansion, giving rise to a pressure transient. In the case of retinal laser treatment, the pressure transient travels through the eye globe and can be measured by means of an ultrasonic transducer, which is gently attached to the eye cornea. Here, the piezo transducer is incorporated with a so-called contact lens.

It can be shown that the amplitude $p_{\max}(T)$ of a pressure transient, originating from tissue at temperature T, is proportional to the tissue absorption coefficient μ_a, the laser radiant exposure H, and the temperature dependent Grüneisen parameter $\Gamma(T)$. It can hence be used to determine the current tissue temperature.

$$p_{\max}(T) \sim \mu_a \cdot H \cdot \Gamma(T) \tag{1}$$

The Grüneisen parameter $\Gamma(T)$ is described by the speed of sound c_s, heat capacity C_p, and density ρ.

$$\Gamma(T) = \frac{1}{\rho(T)} \cdot \frac{\partial \rho(T)}{\partial T} \cdot \frac{c_s(T)^2}{C_p(T)} \tag{2}$$

For water, the main component of soft tissue, the Grüneisen parameter can be approximated by the second order polynomial in the temperature range between T = 10 °C and T = 100 °C:

$$\Gamma(T) \approx \left(T^2 - T_0^2\right) - 2T_{\max}(T - T_0) \tag{3}$$

where T_0 and $T_{\max}$ represent the temperatures where at $p_{\max}$ equals zero, and the maximum of $p_{\max}$, respectively.

The parameters T_0 and $T_{\max}$ are derived by calibration measurements. This is done by measuring pressure transients at different sample temperatures, and plotting the transient amplitudes $p_{\max}$ with respect to sample temperature [13, 19]. T_0 and $T_{\max}$ can then be derived from a numerical fit with Eq. (3) of the measured data. In this work, values of T_0 = –17.0 °C and $T_{\max}$ = 93.3 °C were used, found by Brinkmann et al. [13] for porcine eyes in this manner.

The opto-acoustically probed temperature T_{oa} can finally be computed with the pressure amplitude $p_{\max}$ and laser pulse energy E_{pulse} measured during irradiation using Eq. (4).

$$T_{oa} = T_{\max} - \sqrt{(T_{\max} - T_0)^2 + \frac{p_{\max}}{S \cdot E_{\text{pulse}}}} \tag{4}$$

The proportionality factor S accounts for all unknown eye properties, such as variance in pigmentation, eye lens opacity and transducer characteristics, and is derived during a calibration phase (Section 2.1.3) prior to irradiation of each spot.

The laser energy incident on the RPE is nearly uniformly distributed over the irradiated spot (top-hat profile) and is mostly absorbed in the RPE and choroid according to Beer's law. The temperature value obtained by Eq. (4) subsequently corresponds to a mean depth weighted temperature of the cylindrical volume confined by the beam diameter, its penetration depth, and the widths of the RPE and choroid. Consequently, it is also referred to as volume temperature, $T_{\text{vol}} = T_{oa}$. Due to heat diffusion in the neighboring tissue, the temperature distribution forms a bell-shaped distribution at the surface of the RPE after irradiation duration of approximately 10 ms with an elevated peak temperature T_{peak} in the center of the beam diameter. In earlier work, the elevated peak temperature could be computed by means of a conversion function which was found theoretically by solving the time dependent heat equation [15, 20]. Further details on modeling temperature distribution have been reported by Kleyman et al. [21].

2.1.2 Experimental setup: The RPE is the major absorber at the eyes fundus. Therefore all experiments reported in this paper were conducted on RPE-scleral explants of enucleated porcine eyes, delivered by a local slaughter house. The samples with a diameter of Ø = 12 mm were punched out of the eye fundus and the retina was removed. A simplified sketch of the experimental setup is shown in Figure 1. The upper left part shows an ophthalmological slit lamp (Carl Zeiss Meditec AG, Germany; LSL532s) with integrated laser link, aimed to a sample cuvette with built-in contact lens, which is filled with sodium

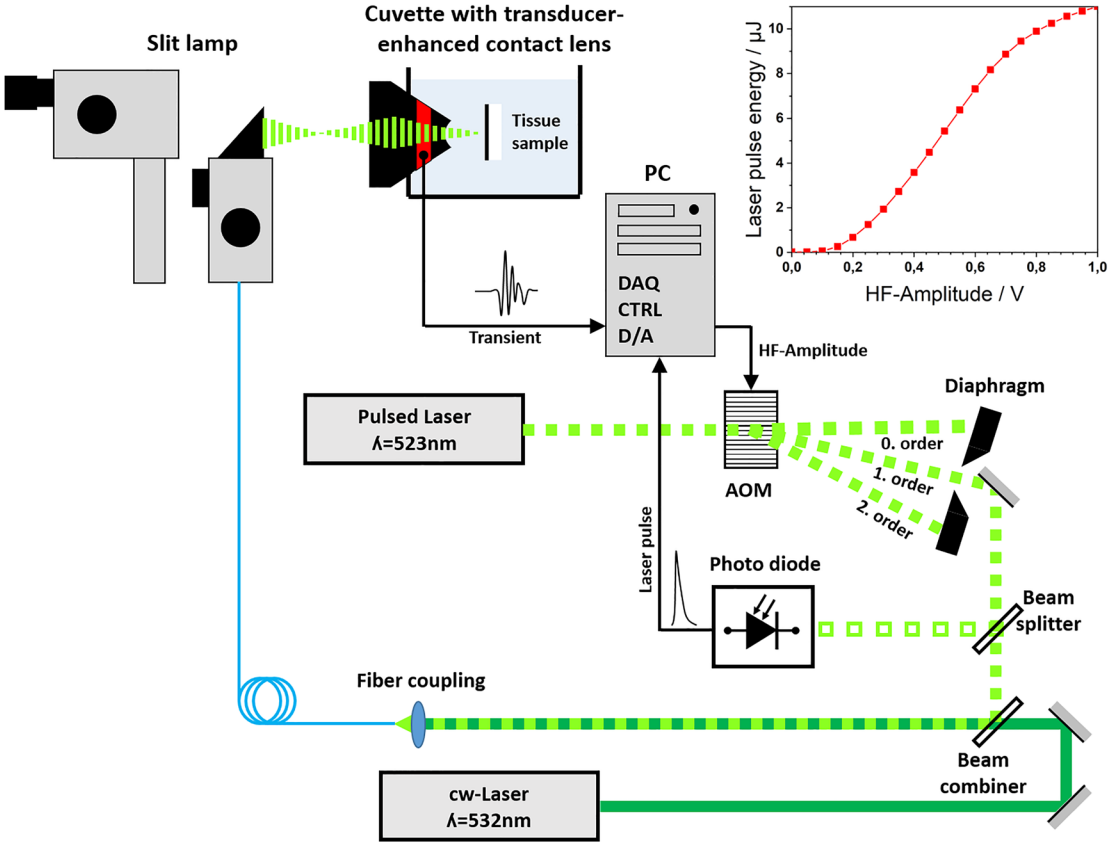

Figure 1: Experimental setup. Ophthalmological slit lamp with sample cuvette, containing transducer enhanced contact lens and RPE sample. Optical setup containing laser, acousto-optic modulator (AOM), photodiode, control PC, and optional cw laser. Inset: Pulse energy calibration.

chloride dilution of 0.9%. A commercial contact lens (Ocular Instruments, USA; Mainster Focal Grid) was customized with a ring-shaped piezo-ceramic transducer with high sensitivity in the MHz frequency range (Medical Laser Center Lübeck, Germany). The irradiated spot diameter was always $Ø_{spot}$ = 200 µm. The distance between the contact lens and the RPE-scleral explants is approximately 23 mm, which corresponds to the typical length of a human eye. To connect the optical setup to the slit lamp, an optical fiber with a core diameter $Ø_{core}$ = 50 µm and numerical aperture NA = 0.1 and SMA terminators at both ends was used.

The lower part of Figure 1 shows a simplified sketch of the optical setup. A Q-switched frequency doubled diode pumped Nd:YLF laser (CrystaLaser, USA; QC-523-100) emitting at λ = 523 nm with a pulse width of τ = 160 ns (FWHM) at a pulse repetition rate of f_{rep} = 10 kHz can be modulated by an acousto-optic-modulator (AOM) (Gooch & Housego, USA; 3080-125) in order to distribute the laser energy to higher orders of diffraction. Here, only the first order of diffraction is used for sample irradiation. The amount of energy is set by modulating the HF-Amplitude between U_{HF} = 0 V and U_{HF} = 1 V by means of a digital to analog converter (D/A) (National Instruments, USA; PCIe-6341). For calibration, the laser pulse energy was measured as a function of U_{HF} in steps of ΔU_{HF} = 50 mV between the slit lamp and contact lens using an energy meter (Coherent, USA; USB J-10MT-10 kHz) (inset Figure 1). The maximum pulse energy measured here was $E_{pulse,max}$ = 11 µJ, corresponding to a maximum optical power of $P_{opt,max}$ = 110 mW at f_{rep} = 10 kHz repetition rate. During irradiation, pulse energy can be set by means of linear interpolation between measured calibration voltages with a resolution of ΔU_{HF} = 15.3 mV.

Prior to fiber coupling a small portion of the beam energy of approximately 0.5% is coupled to a pre-amplified photodiode (Thorlabs Inc., USA; PDA10A2) using a beam splitter (Thorlabs Inc., USA; WW41050-A). This allows for normalizing the pressure transients to the applied laser pulse energy E_{pulse}; as result, this compensates for laser pulse energy fluctuations (Eq. (4)). A fast data acquisition board (DAQ) (Vitrek, LLC, USA; GaGe CSE4347) in the PC simultaneously records both, laser pulses and pressure transients at a sampling rate of 100 MS/s. The transient voltage signal is additionally amplified by two preamplifiers prior to recording (not shown in Figure 1). The first one (Olympus/Panametrics, Japan; 5660B) amplifies the signal by a factor of 1000, and the second one (Stanford Research Systems, USA; SR5660B) amplifies the signal by a factor of 10 and applies a bandwidth filter of 10 kHz to 1 MHz to the transient signal. Figure 2 exemplarily shows typical transient and pulse signals recorded in this manner. The entire setup is controlled by software with graphical user interface written in the MS visual C++/MFC language.

In order to compare pulsed and continuous wave (cw) tissue heating and temperature courses, a commercial ophthalmic treatment laser beam (Carl Zeiss Meditec AG, Germany; Visulas 532s) was collinearly superimposed with the pulsed beam by means of a dichroic mirror (Figure 1). Since the cw laser cannot be controlled in real-time in the current setup an open loop comparison at predefined same average power was performed.

2.1.3 Signal processing and measurement scheme: Figure 2 illustrates measurements of a transient and the respective laser pulse. In order to compute the tissue temperature using Eq. (4), the measurements of the transient and the pulse as shown in Figure 2 have to be converted into the scalar values p_{max} and E_{pulse}. Instead of retrieving the maximum amplitude of the transient, the sum of absolute sample voltages $U_{Transducer}$ over some time was used.

$$p_{max} \cong \sum_{t=t_0}^{t_0+\Delta t} |U_{Transducer}(t)| \tag{5}$$

Here, a duration of Δt = 10 µs (i.e. 1000 samples at 100 MS/s) was used in the range highlighted in yellow in Figure 2(A). The value of E_{pulse} was derived in the same manner from the laser pulse measurement for Δt = 1 µs in the highlighted range in Figure 2(B). The delay between the laser pulse and the beginning of the transient depends on the distance between the piezo transducer and the sample with respect to the speed of sound of the medium within. Besides the duration of the summation for both signals, the starting point t_0 is settled from the measurement software.

Figure 3 shows a scheme of the current measurement method. In this work, a laser repetition rate of f_{rep} = 10 kHz was used. However, to ensure real-time processing of the extensive MPC-algorithm, the

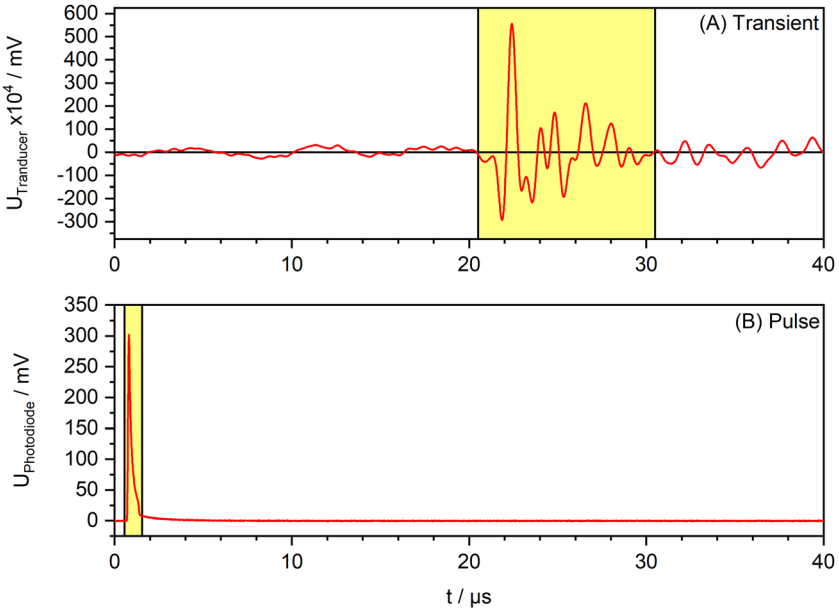

Figure 2: Typical measured signals. Top: Transient, bottom: Pulse. Parts highlighted in yellow correspond to the ranges used for temperature computation.

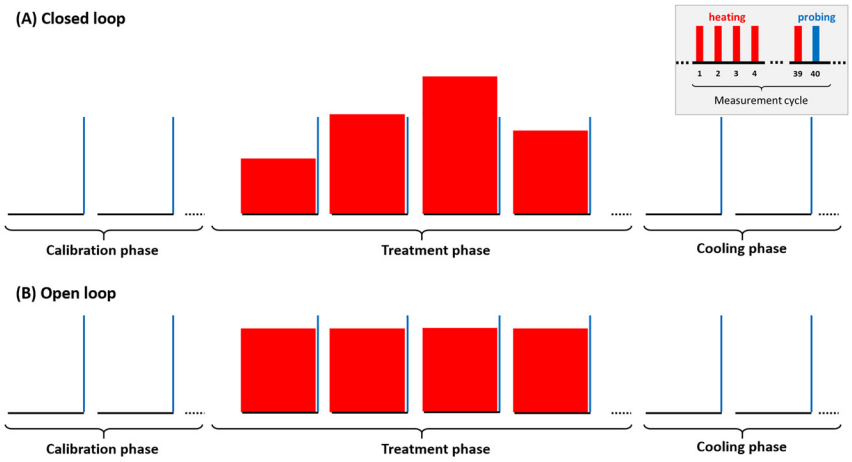

Figure 3: Measurement scheme for 250 Hz probing.
(A) Closed loop, controlled. (B) Open loop, irradiation with fixed laser pulse energy. Probing pulses are drawn in blue, heating pulses in red. The inset shows a single measurement cycle in detail.

probing rate was restricted to $f_{\text{probe}} = 250$ Hz. At the beginning of each measurement cycle, 39 subsequent pulses of equal energy were used for tissue heating. The 40th pulse was used for temperature probing, as indicated in the inset in Figure 3 for a single measurement cycle. The pulse energies for heating and probing pulses can be set individually by the AOM. For open loop experiments, heating and probing pulse energies were kept constant over the entire measurement (Figure 3(B)). For closed loop experiments, the probe pulse energy was kept constant over the entire measurement, while the heating pulse energy was changed for each measurement cycle by the control algorithm (Figure 3(A)). The average optical power P_{avr} over one measurement cycle applied to the tissue over one measurement cycle can be computed as

$$P_{\text{avr}} = \left[\left(\frac{f_{\text{rep}}}{f_{\text{probe}}} - 1\right)E_{\text{heat}} + E_{\text{probe}}\right] \cdot f_{\text{probe}} \tag{6}$$

with the laser repetition rate f_{rep}, the measurement rate f_{probe} and the laser pulse energies E_{probe} and E_{heat} used for probing and heating, respectively.

The entire irradiation of a single spot can be divided into three phases. The calibration phase at the beginning of the treatment is used to derive the proportionality factor S (refer to Section 2.1.1) which is different for each spot and is needed for computing the temperature in the actual treatment phase using Eq. (4). The factor S is derived from Eq. (4) using $T = T_{\text{body}}$, the body temperature of the treated person in clinical application. In case of working with explanted porcine samples, T_{body} is set to the dilution temperature in the cuvette which was equal to room temperature, here $T_{\text{body}} = 21$ °C.

During the calibration phase, S is measured 15 times and the mean value is used to compute the temperature in the treatment phase. Here, heating pulses are suppressed by the AOM and probe pulse energy is set to $E_{\text{probe}} = 3.0$ µJ. At the probing frequency of $f_{\text{probe}} = 250$ Hz the temperature increase during calibration phase is assumed to be negligible [19]. During the treatment phase, the laser power is either precomputed (open-loop) or is computed by the controller at each time step based on the measured temperature (closed-loop). The cooling phase at the end of the treatment is optional and can be used to monitor the cooling of the tissue after heating. During the cooling phase, heating pulses are suppressed as well.

For the comparison of pulsed and cw tissue temperature courses, the heating pulses were completely suppressed during the heating phase ($E_{\text{heat}} = 0$) and the cw laser was enabled instead. The combined laser power P_{comb} incident on the tissue sample therefore is the sum of the settled cw laser power and the pulsed average power with respect to the probe energy E_{probe} and probe frequency f_{probe}:

$$P_{\text{comb}} = P_{\text{cw}} + P_{\text{probe}} = P_{\text{cw}} + E_{\text{probe}} \cdot f_{\text{probe}} \tag{7}$$

2.2 State estimation, parameter identification, and control

In this section, the overall control scheme is described. An extended Kalman-filter (EKF) is utilized to estimate the state and the absorption coefficient and a model predictive controller (MPC) to adjust the laser power. Figure 4 shows a block diagram of the whole system. The volume temperature $T_{\text{vol}} = T_{\text{oa}}$ is calculated based on Eq. (4). This volume temperature is then used to estimate the state, i.e., the temperature distribution at the heated spot, and the parameters, i.e., the absorption coefficients. As the EKF needs some settling time for the parameter to converge to a certain value, the treatment is divided into two phases – identification phase and control phase. During the identification phase the laser power u is set to some prearranged constant. In the control phase, the states and parameter estimates $\hat{x}$ and $\hat{\mu}$ are passed on to the MPC that computes the laser power that is needed to reach and stay at the desired peak temperature $T_{\text{peak, }d}$.

2.2.1 State estimation and parameter identification: In order to allow for model predictive control, the internal states and parameters of the model need to be known. Hence, the states and the strongly spot-dependent absorption coefficient μ are estimated. An EKF for joint state and parameter estimation is used. The EKF is a well-known state observer for nonlinear systems, see e.g. [22]. It is based on a successive

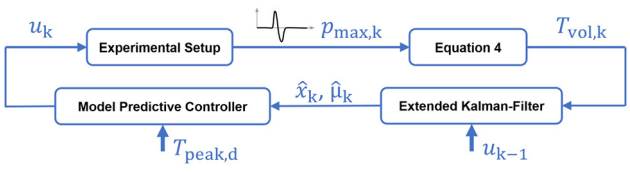

Figure 4: Block diagram of the closed-loop system.

linearization of a nonlinear model that is subject to uncorrelated and normally distributed process and measurement noise.

The modeling, starting from the infinite-dimensional heat diffusion equation, to a low-dimensional state-space model is briefly described in the following, for details see [18, 21]. The basis for the model is the partial differential equation (PDE) of the heat diffusion. The PDE is spatially discretized by finite differences which leads to a high dimensional, continuous-time model. As this model remains too large for real-time estimation and (model-based) control, the model order is reduced. A parametric model order reduction in [23] was utilized and the approach was generalized for our purposes to preserve the parameter dependency of the absorption coefficient in [21]. Finally, the reduced order model is discretized in time to obtain a discrete-time state-space model

$$x_{k+1} = Ax_k + B(\mu_k)u_k \tag{8}$$
$$y_k = C(\mu_k)x_k \tag{9}$$

with $\mathrm{A} \in R^{n\times n}$, $\mathrm{B}(\mu) \in R^{n\times 1}$, $\mathrm{C}(\mu) \in R^{2\times n}$ with state dimension n. Here, the output y is the peak and the volume temperature, i.e. $y = [C_{\mathrm{vol}}(\mu)x, C_{\mathrm{peak}}x]^\top = [T_{\mathrm{vol}}, T_{\mathrm{peak}}]^\top$. It is important to note that the output of the system that can be measured in practice, is only the volume temperature T_{vol}. However, the relationship between the states and the peak temperature T_{peak} is needed for MPC since the peak temperature determines and dominates biochemical reaction rates in the tissue. Consequently, it is considered as an output for the model order reduction, which is only used for control but not for state and parameter estimation. To enable parameter estimation, the state-space is extended by the time-invariant but spot-dependent absorption coefficient, i.e. $\mu_{k+1} = \mu_k$, which leads to a nonlinear model that is used for the estimation of the states and the parameter.

2.2.2 Model predictive control: Model predictive control (MPC) is an iterative optimization-based control technique. The basic idea of MPC is to make use of a dynamical system to forecast and optimize the behavior of the system [24]. The advantages of MPC include the capacity to handle constraints such as the maximum laser power and maximum peak temperature. At time t, the current state is measured and a control input minimizing some objective function is computed for a future time horizon $[t, t+N]$.

In the present setting, the objective is to compute online a sequence of optimal laser power, with a set maximum power, to attain a desired peak temperature, based on the evolution of the states. Based on the measured current state x_t, the sequence of N future states

$$x = (x_t, \ldots, x_{t+N}) \tag{10}$$

and optimal laser power to drive the state closer to the desired point—the state that renders the reference peak temperature—in time $t+N$ is obtained as the solution of an optimization problem as follows.

Recall the dynamical system is given by Eq. (8) and

$$y_{\mathrm{peak},k} = C_{\mathrm{peak}}x_k \tag{11}$$

The objective function

$$J(x,u) = \sum_{k=t}^{t+N-1} \left(C_{\mathrm{peak}}x_k - y_{\mathrm{ref}}\right)^\top Q\left(C_{\mathrm{peak}}x_k - y_{\mathrm{ref}}\right) + u_k^\top R u_k \tag{12}$$

is defined to measure the deviation from the desired output value y_{ref}. Let the control sequence

$$u = (u_t, \ldots, u_{t+N-1}) \tag{13}$$

be a solution of the optimization problem

$$\min_u J(x,u) \tag{14}$$

subject to

$$x_{k+1} = Ax_k + B(\mu_k)u_k \tag{15a}$$
$$x_t = \hat{x}_t \tag{15b}$$
$$C_{\mathrm{peak}}x_k \le T_{\mathrm{peak,\,max}} \tag{15c}$$
$$u_k \in [0, u_{\max}] \;\forall\; k = t \ldots t+N-1 \tag{15d}$$

Then, the first element u_t of the solution sequence is used as the control of the system at time t before the time horizon is shifted and the optimization step is repeated.

The MPC scheme assumes that states are known or can be measured, which poses a challenge in the present setting as only the volume temperature T_{vol} is available. In the present application, an EKF is used to estimate the initial states and the parameters required for the solution of Eq. (15).

3 Results

In order to demonstrate the equality of pulsed and cw tissue heating, Figure 5 shows open loop temperature measurements of the volume temperature T_{vol} using pulsed only and combined pulsed and cw irradiation. Both temperature progressions were measured using moving averaging over four single measurements and probe energies of $E_{\mathrm{probe}} = 4$ µJ. The heating energy for the pulsed only measurement was $E_{\mathrm{heat}} = 6.22$ µJ, the cw laser power for the combined measurement was $P_{\mathrm{cw}} = 56$ mW. Using Eqs. (6) and (7) this yields a total irradiation power of $P = 60$ mW in each case with a probe frequency of $f_{\mathrm{probe}} = 1$ kHz. Starting

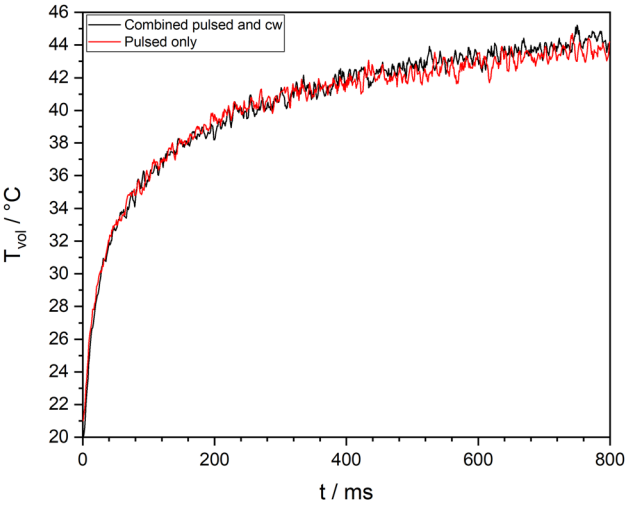

Figure 5: Comparison of open loop temperature measurements by means of pulsed only and combined pulsed and cw tissue irradiation at $P = 60$ mW total laser power in each case.

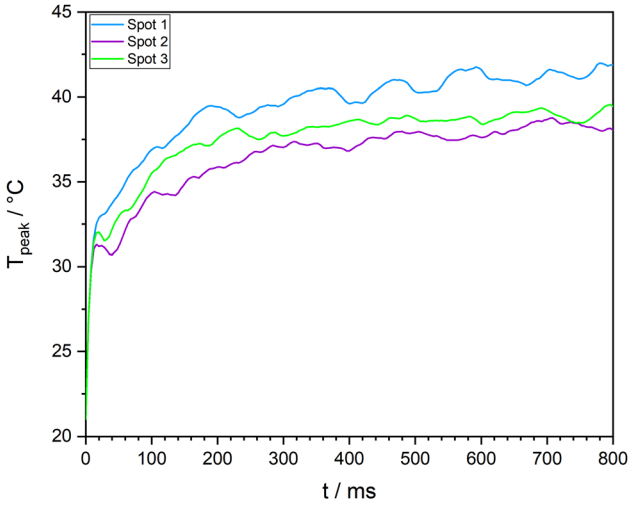

Figure 6: Peak temperatures at different spots of the irradiated RPE sample with a laser power of 20.25 mW.

at reference temperature T_{ref} = 21 °C, both measurements nearly show the same progression and a volume temperature of T_{vol} = 44 °C after t = 800 ms which implies the equality of pulsed and cw tissue heating.

In the following passage, first results of the closed-loop control with EKF and MPC in combination with opto-acoustic temperature measurement are presented. To motivate the model-based approach, the open-loop experiments were conducted with a constant probe energy of E_{probe} = 3 µJ and constant heat energy E_{heat} = 2 µJ, which corresponds to a constant average laser power of P_{avr} = 20.25 mW (Eq. (6)). Figure 6 shows the peak temperature at three different spots at the RPE-sclera explants that have been irradiated with the same laser power. The peak temperature increase is different for each spot as the absorption varies from spot to spot.

In comparison, Figure 7 shows closed-loop experiments at different spots. Figure 7(A) shows a controlled temperature progression using MPC. For solving the optimal control problem, the solver *OSQP* [25] is used. The desired peak temperature increase y_{ref} is 20 °C, which corresponds to a peak temperature of 41 °C with respect to a base temperature of 21 °C. In the identification phase (first 396 ms) the laser power is constantly at P_{avr} = 20 mW, cf. Figure 7(B). The temperature increase is similar to the open-loop experiment. Depending on the absorption, the peak temperature increase differs. As soon as the controller is turned on (t > 396 ms), the temperature increases at all spots and reaches 41 °C. Between 440 ms and 800 ms the mean of the absolute error between the desired peak temperature and the achieved peak temperature is 0.05 °C (blue), 0.08 °C (green), and 0.1 °C (purple). These first real-time ex vivo experiments show promising results and motivate further investigations of the control strategy, also with respect to faster sampling rates in the control cycle.

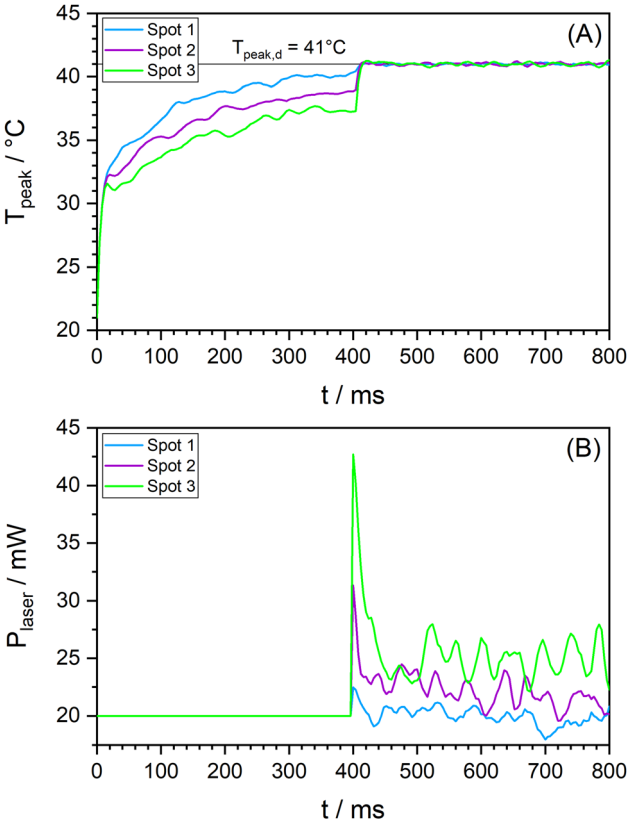

Figure 7: Peak temperature at different spots of the RPE sample (A), and laser power during identification phase (396 ms) and closed-loop control (400–800 ms) (B).

4 Summary and discussion

In this paper a 10 kHz pulsed laser setup for temperature-controlled retinal laser irradiation has been presented, providing a maximum optical average power of 110 mW. The equality of pulsed and continuous wave (cw) tissue heating and temperature progression was shown at a total incident average laser power of 60 mW, using probing energies of 4 µJ at a repetition rate of 1 kHz in each case. The pulse energy used for solely pulsed heating with 10 kHz was 6.22 µJ. The setup has shown its capability to heat irradiated spots on enucleated porcine RPE-scleral explants to a predefined aim temperature of 41 °C and maintain the temperature for 400 ms with an accuracy of ±0.1 °C, regardless varying RPE pigmentation at different spots, by means of opto-acoustic temperature measurement and model predictive control.

Nevertheless, more extensive investigations including cell vitality will be performed in the future, especially for heating with pulse energies higher than 10 µJ.

The setup presented here for opto-acoustic temperature measuring during retinal laser treatment requires less technical effort compared to earlier approaches [9], which extensively incorporated a conventional medical treatment laser, which continuously emits laser light during irradiation. Hence, this approach enables the development of more economical retinal treatment devices with sophisticated opto-acoustic temperature control for ophthalmology.

In this work, separate laser pulse energies for probing and heating were used during the entire irradiation process. This scheme enables using comparatively high probe pulses to obtain good signal to noise ratio and low energy heating pulses for gentle tissue heating. In the future, with improved hardware and performance optimized control algorithms, it is envisaged to enable pulse to pulse control at sampling rates of 10 kHz and more.

On the other hand, the modulation scheme used so far can be used with higher pulse repetition rates and lower heating pulse energies to enable smoother tissue heating to make this technique comparable to cw heating. However, the maximum laser repetition rate is limited to approximately 50 kHz due to the duration and transit time of a pressure transient. At higher repetition rates, subsequent transients would overlap and frustrate temperature measurement.

Opto-acoustic temperature control was first used to automatically interrupt irradiation when a predefined aim temperature was reached (open-loop) [9]. Later, PID-controllers were used to quickly reach and maintain the aim temperature for a specified time [16, 17]. PID parameters were found by means of the H_∞-method which provides robust control, even for varying conditions in the eye, providing fast control rates of up to 1 kHz. In this work, sophisticated model predictive control algorithms have been used which provide even more reliable control since MPC can explicitly consider constraints in the control design. But MPC also requires more computational effort. In this preliminary phase of this project a sampling rate of 250 Hz was used to ensure real-time control due to the computational expenses of the optimization-based (model predictive) controller. However, faster sampling rates with faster hardware and optimization of control algorithms are purpose of current work and promise to compete with the speed of other approaches reported so far and achieve even more reliable and secure temperature control. These first closed-loop results using MPC can consequently be seen as a proof of concept for the model-based control approach to ensure more reliable and safer treatment.

Acknowledgments: We also gratefully acknowledge C. Kren and V. Danicke from the Medical laser Center Lübeck for supporting this work.

Author contributions: All the authors have accepted responsibility for the entire content of this submitted manuscript and approved submission.

Research funding: This work is funded by the German Research Foundation (DFG) under the project number 430154635 (MU 3929/3-1, WO 2056/7-1, BR 1349/6-1).

Conflict of interest statement: The authors declare no conflicts of interest regarding this article.

References

[1] Early Treatment Diabetic Retinopathy Study Research Group, "Early photocoagulation for diabetic retinopathy," *Ophthalmology*, vol. 98, no. 5, pp. 766–785, 1991.

[2] Early Treatment Diabetic Retinopathy Study Research Group, "Photocoagulation for diabetic macular edema," *Arch. Ophthalmol.*, vol. 103, pp. 1796–1806, 1985.

[3] A. M. Shah, N. M. Bressler, and L. M. Jampol, "Does laser still have a role in the management of retinal vascular and neovascular diseases?" *Am. J. Ophthalmol.*, vol. 152, no. 3, pp. 332–339.e1, 2011.

[4] The Central Vein Occlusion Study Group, "Natural history and clinical management of central retinal vein occlusion," *Arch. Ophthalmol.*, vol. 115, pp. 486–491, 1997.

[5] Branch Vein Occlusion Study Group, "Argon laser scatter photocoagulation for prevention of neovascularization and vitreous hemorrhage in branch vein occlusion. A randomized clinical trial. Branch Vein Occlusion Study Group," *Arch. Ophthalmol.*, vol. 104, pp. 34–41, 1986.

[6] G. Meyer-Schwickerath, "Licht Koagulation, eine Methode zur Behandlung und Verhuetung der Netzhautabloesung," *Albrecht Von Graefes Arch. Ophthalmol.*, vol. 156, no. 1, pp. 2–34, 1954.

[7] S. Arrhenius, "Über die Reaktionsgeschwindigkeit bei der Inversion von Rohrzucker durch Säuren," *Z. Phys. Chem.*, vol. 4U, no. 1, pp. 226–248, 1889.

[8] D. Lavinsky and D. Palanker, "Nondamaging photothermal therapy for the retina: initial clinical experience with chronic central serous retinopathy," *Retina*, vol. 35, no. 2, pp. 213–222, 2015.

[9] A. Baade, C. von der Burchard, M. Lawin, et al., "Power-controlled temperature guided retinal laser therapy," *J. Biomed. Opt.*, vol. 22, no. 11, pp. 1–11, 2017.

[10] M. L. Denton, G. D. Noojin, M. S. Foltz, et al., "Spatially correlated microthermography maps threshold temperature in laser-induced damage," *J. Biomed. Opt.*, vol. 16, no. 3, p. 36003, 2011.

[11] S. Y. Schmidt and R. D. Peisch, "Melanin concentration in normal human retinal pigment epithelium. Regional variation and age-

related reduction," *Investig. Ophthalmol. Vis. Sci.*, vol. 27, no. 7, pp. 1063–1067, 1986.
[12] W. J. Geeraets, R. C. Williams, G. U. Chan, W. T. Ham, Jr, D. Guerry, III, and F. H. Schmidt, "The relative absorption of thermal energy in retina and choroid," *Investig. Ophthalmol. Vis. Sci.*, vol. 1, no. 3, pp. 340–347, 1962.
[13] R. Brinkmann, S. Koinzer, K. Schlott, et al., "Real-time temperature determination during retinal photocoagulation on patients," *J. Biomed. Opt.*, vol. 17, no. 6, p. 61219, 2012.
[14] K. Schlott, S. Koinzer, A. Baade, R. Birngruber, J. Roider, and R. Brinkmann, "Lesion strength control by automatic temperature guided retinal photocoagulation," *J. Biomed. Opt.*, vol. 21, no. 9, p. 98001, 2016.
[15] K. Schlott, S. Koinzer, L. Ptaszynski, et al., "Automatic temperature controlled retinal photocoagulation," *J. Biomed. Opt.*, vol. 17, no. 6, p. 61223, 2012.
[16] C. Herzog, O. Thomsen, B. Schmarbeck, M. Siebert, and R. Brinkmann, "Temperature-controlled laser therapy of the retina via robust adaptive H_∞-control," *Automatisierungstechnik*, vol. 66, no. 12, pp. 1051–1063, 2018.
[17] H. S. Abbas, C. Kren, V. Danicke, C. Herzog, and R. Brinkmann, "Toward feedback temperature control for retinal laser treatment," in *Medical Laser Applications and Laser-Tissue Interactions IX*, Translation of Lasers and Biophotonics Technologies and Procedures: Toward the Clinic, L. D. Lilge and C. M. Philipp, Eds., Munich, Germany, SPIE, 2019, p. 10.
[18] V. Kleyman, M. Schaller, M. Wilson, et al., "State and parameter estimation for model-based retinal laser treatment," in *7th IFAC Conference on Nonlinear Model Predictive Control 2021*, 2021.
[19] J. Kandulla, H. Elsner, R. Birngruber, and R. Brinkmann, "Noninvasive optoacoustic online retinal temperature determination during continuous-wave laser irradiation," *J. Biomed. Opt.*, vol. 11, no. 4, p. 41111, 2006.
[20] R. Birngruber, F. Hillenkamp, and V. P. Gabel, "Theoretical investigations of laser thermal retinal injury," *Health Phys.*, vol. 48, pp. 781–796, 1985.
[21] V. Kleyman, H. Gernandt, K. Worthmann, H. S. Abbas, R. Brinkmann, and M. A. Müller, "Modeling and parameter identification for real-time temperature controlled retinal laser therapies," *Automatisierungstechnik*, vol. 68, no. 11, pp. 953–966, 2020.
[22] C. K. Chui and G. Chen, *Kalman Filtering*, Cham, Springer International Publishing, 2017.
[23] U. Baur, C. Beattie, P. Benner, and S. Gugercin, "Interpolatory projection methods for parameterized model reduction," *SIAM J. Sci. Comput.*, vol. 33, no. 5, pp. 2489–2518, 2011.
[24] J. B. Rawlings, D. Q. Mayne, and M. M. Diehl, *Model Predictive Control: Theory, Computation, and Design*, 2nd ed. Santa Barbara, CA, USA, Nob Hill Publishing, LLC, 2019.
[25] B. Stellato, G. Banjac, P. Goulart, A. Bemporad, and S. Boyd, "OSQP: an operator splitting solver for quadratic programs," *Math. Prog. Comp.*, vol. 12, no. 4, pp. 637–672, 2020.